Supplement of Atmos. Chem. Phys., 21, 15809–15826, 2021
https://doi.org/10.5194/acp-21-15809-2021-supplement

Atmospheric Chemistry and Physics
Open Access
EGU

Supplement of

Improving the representation of HONO chemistry in CMAQ and examining its impact on haze over China

Shuping Zhang et al.

Correspondence to: Golam Sarwar (sarwar.golam@epa.gov), Jia Xing (xingjia@tsinghua.edu.cn), and Hong He (honghe@rcees.ac.cn)

Selection of uptake coefficients

The selection of uptake coefficients on ground surface and aerosol surface are mainly based on the empirical data. And we also referred to some experimental data measured in our laboratory. Experimental data measured on MgO surface fall in the range of $1\text{-}6\times10^{-6}$ as reported by Ma et al. (2017) and on hematite surface in the range of 1.9×10^{-7}-1.6×10^{-6} as reported by Liu et al. (2015) . The derived empirical data obtained by VandenBoer et al. (2013) from the field observation fall in the range of 2×10^{-6} -1.6×10^{-5}. The empirical uptake coefficient used in models varied widely ranging from 10^{-7} to 10^{-3} (Table S2). The majority γ_{NO2} value employed in literature is about 10^{-6}.

Calculation of dry deposition velocities

The total resistance to dry deposition (which is the inverse of v) is calculated as the sum of the bulk surface resistance, R_{surf}, the aerodynamic resistance, R_a, the quasi-laminar

boundary layer resistance, R_{bc}. Rsurf includes the influence of vegetation, canopy, ground, etc. Considering the average temperature in our study is around 1.6 ℃,we used the default mechanism of the surface resistance in CMAQ without modification for low temperatures as suggested in Jaegle's method (-2℃) (Jaeglé et al., 2018),. However, our model calculated deposition velocities fall within the reported ranges of values (Jaeglé et al., 2018). The modeling value of v(HNO_3) falls within the range of 3×10^{-4} cm s^{-1} to 4.1cm s^{-1} with an average velocity of 0.5 cm s^{-1}. The simulated value of v(HCl) falls in 1×10^{-4} cm s^{-1} to 0.1 cm s^{-1} with an average velocity of 0.02 cm s^{-1}.

$$v = (R_{surf} + Ra + R_{bc})^{-1}$$

$$R_{bc} = \frac{5}{v(\frac{k}{d})^{\frac{2}{3}}}$$

v is the cell friction velocity (m/s); k is kinematic viscosity(cm^2/s); d is molecular diffusivity (cm^2/s);

Sensitivity analysis

Six additional model sensitivity simulations were performed to better understand the impacts of selected parameters on HONO predictions. One simulation was to investigate the sensitivity of the selected night-time uptake coefficient for the heterogeneous reaction of NO_2 on ground surface by doubling the uptake coefficient (from 4×10^{-6} to 8×10^{-6}). It substantially increases the night-time HONO predictions and seriously overestimates the observed HONO concentration (Fig. S3). To investigate the impact of the selected aerosol nitrate photolysis rate, the second simulation was performed by increasing the aerosol nitrate photolysis rate from 30×HNO_3 photolysis rate to 100×HNO_3 photolysis rate. It marginally increases the predicted (12:00 to 18:00) HONO in the afternoon concentrations from 0.72 ppb to 0.82 ppb (Fig. S3). Model underestimates daytime NO_2 concentrations, which can lower the model daytime of HONO concentrations. Planetary boundary layer (PBL) height affects model daytime concentration. However, PBL height could not be evaluated because it was not measured. To investigate the causes of daytime HONO underestimation, the third sensitivity simulation was performed by doubling the NO_x emissions. The underestimation of the NO_x concentration in the afternoon decreases from 39 ppb to 36 ppb, whereas the simulated HONO concentrations in the afternoon (12:00 to 18:00) increases from 1.0 ppb to 2.4 ppb (Fig. S3). Another possible reason of daytime HONO underestimation is the overestimation of daytime photolysis reaction rate. Aerosols in heavy pollution periods can reduce the amount of radiation reaching the ground and can lower the photolysis reaction rate. The last sensitivity simulation was conducted by reducing the photolysis rate by 50%. The daytime HONO concentration increases from 1.3 to 2.1 ppb, which improves the comparison with observed data (Fig. S3). Chemical kinetics of R2 and R3 (Table 1) in CB6 are based on the results of Kaiser and Wu (1977) which are lower than the values reported by Chan et al. (Chan et al., 1976a; Chan et al.,

1976b). We also performed a separate simulation by using the higher rate constants reported by Chan et al. (1976a, 1976b) (Fig. S4). As expected, the use of higher rate constants did not change predicted HONO concentrations appreciably which reiterates that the contribution of gas-phase chemistry to HONO concentration is relatively small. S/Vg was set to 2.2/H in another sensitivity case. The average HONO increased by 17.2% (from 2.5 ppb with 1.7/H (HONO_REV) to 2.9 ppb with 2.2/H). Results of our sensitivity analyses reveal that the daytime HONO underestimation can be improved by solving the problem of daytime NO_2 underestimation (Fig. S5) and improving the HONO photolysis reaction rates. Future studies can target on such improvements.

Except the six parameterized reactions, the photolysis of deposited HNO_3, soil emission and traffic emission are other potential HONO sources. Zhou et al., (2003) reported that HNO_3 deposited on environmental surfaces can undergo rapid photolysis leading to day-time HONO production. Several studies (Sarwar et al., 2008; Fu et al., 2019; Liu et al., 2019b) included such a reaction in their models. However, we do not include it because the rate constant has high uncertainty and it could also pose a problem for performing long-term model simulations. For long-term (annual and multiyear) simulation, that the deposited amount of HNO_3 could accumulate with time, which could continue increasing the HONO production rates with time. Soil can emit HONO and other nitrogen-containing compounds (Su et al., 2011; Oswald et al., 2013). Rasool et al. (2019) implemented these emissions into CMAQv5.3 by using a mechanistic representation of the underlying processes and examined their impacts on air quality over North America. The impacts of HONO emitted from soil are generally low, and we do not include these emissions in this study. Traffic emissions are usually estimated from the ratio of $HONO/NO_x$, ranging from 0.3% to 2.1% (Kurtenbach et al., 2001; Svoboda et al., 2013; Czader et al., 2015; Wormhoudt et al., 2015; Xu et al., 2015; Liang et al., 2017; Nakashima and Kajii, 2017; Trinh et al., 2017; Rasool et al., 2019). The $HONO/NO_x$ emission ratio used in CMAQv5.3 (0.8%) falls within the reported ranges. Some researchers classify the reaction between vehicle-emitted NO and OH as traffic source. Our research emphasizes the contribution of each chemical reaction including NO+OH, and does not investigate the differences in traffic sources. We also applied our parameter method into another case at Wangdu in winter of 2017. The simulated HONO improves remarkably (Zheng et al., 2020).

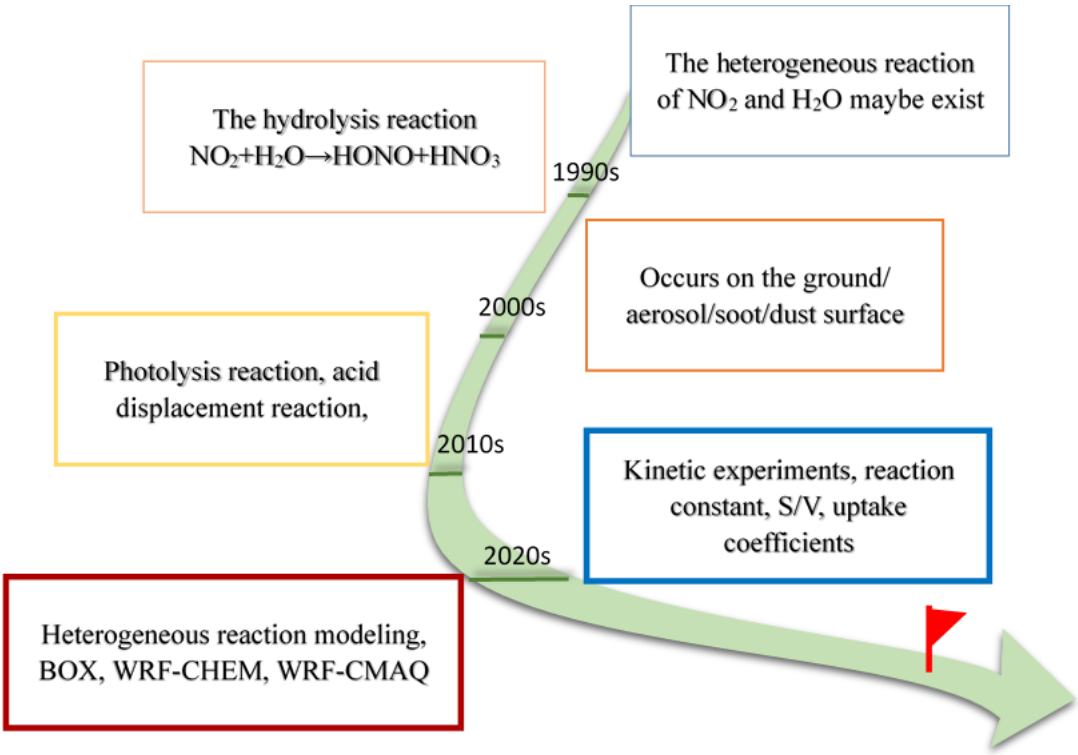

Fig. S1 Research history of HONO heterogeneous reactions in past decades

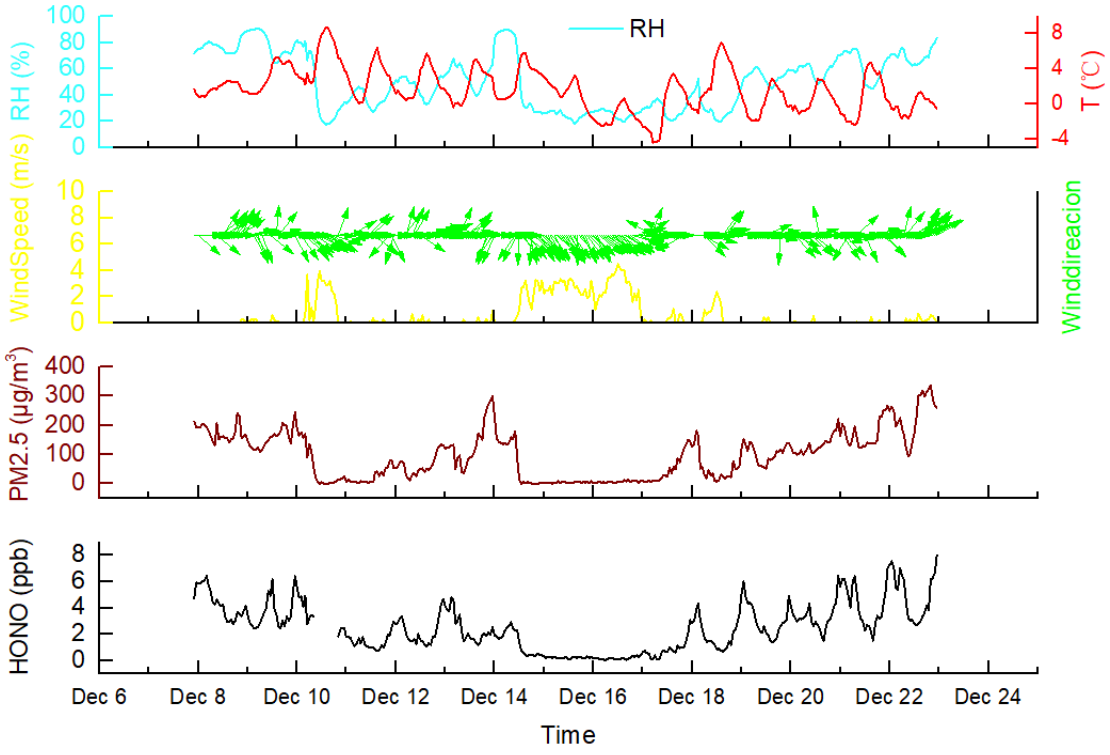

Fig. S2: Observed temperature, relative humidity (RH), wind speed, wind direction, $PM_{2.5}$, and HONO concentrations in Beijing in December 2015.

.

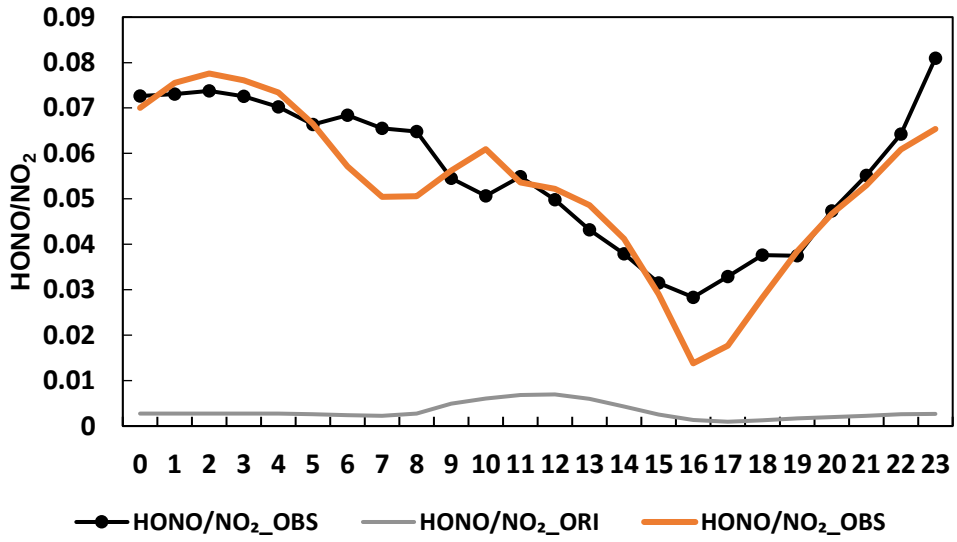

Fig. S3: Average diurnal variation of $HONO/NO_2$ during 7-22 December in Beijing.

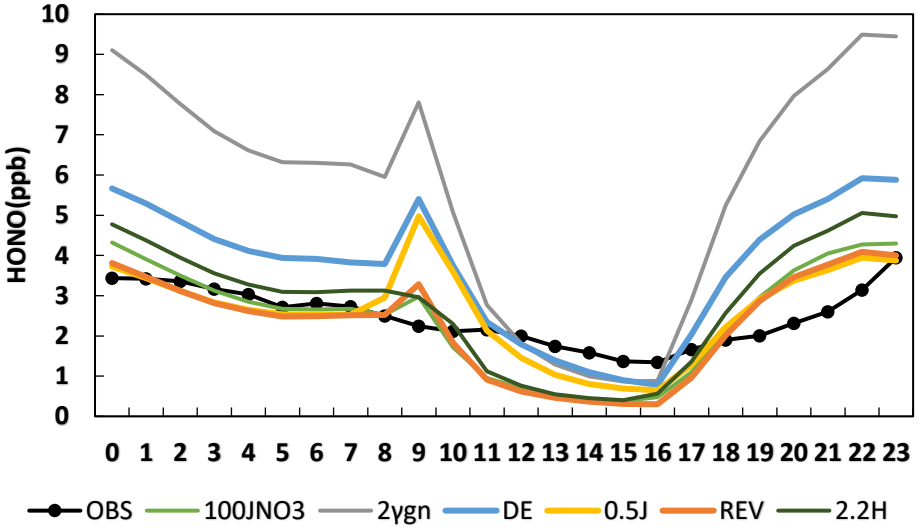

Fig. S4: Diurnal variation of sensitivity simulations during 7-22 December in Beijing. HONO observation is denoted as OBS, final simulated HONO concentration is denoted as REV, HONO with nitrate photolysis rate of 100×JHNO3 is denoted as 100JNO3, HONO with 2×γgn is denoted as 2γgn, HONO concentration with double NO_x emission is denoted as DE, HONO with 2.2/H is denoted as 2.2H and HONO with one-half of the photolysis rate is denoted as 0.5J.

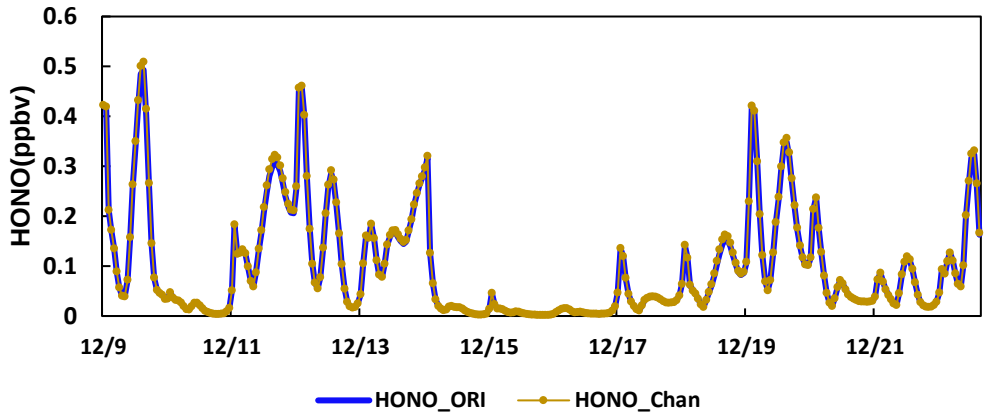

Fig.S5 HONO simulated by default rate coefficients in CB6 (denoted by HONO_ORI) and that measured by Chan et al (1976) (denoted by HONO_Chan).

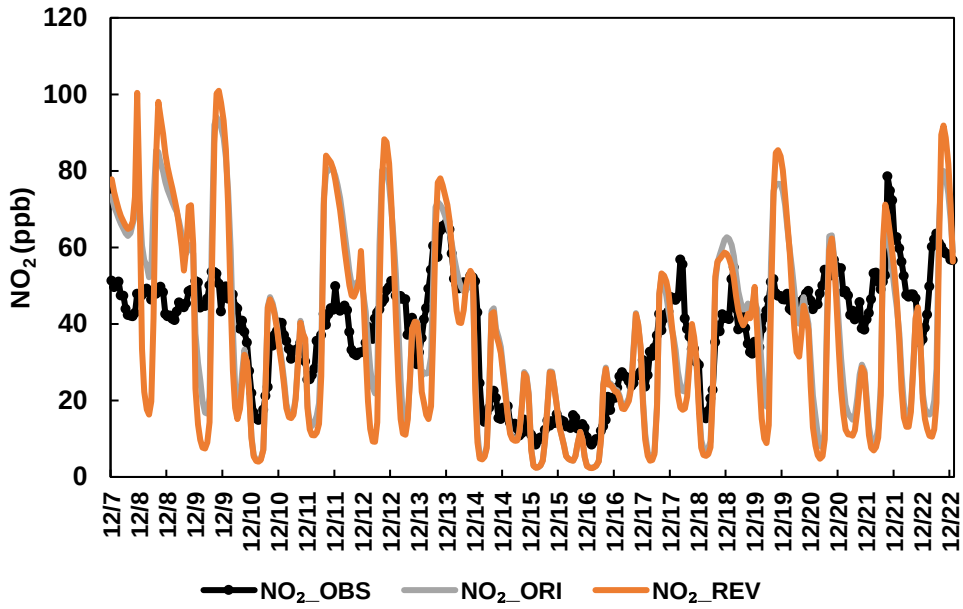

Fig. S6: A comparison of observed and simulated NO_2 in Beijing (hourly data).

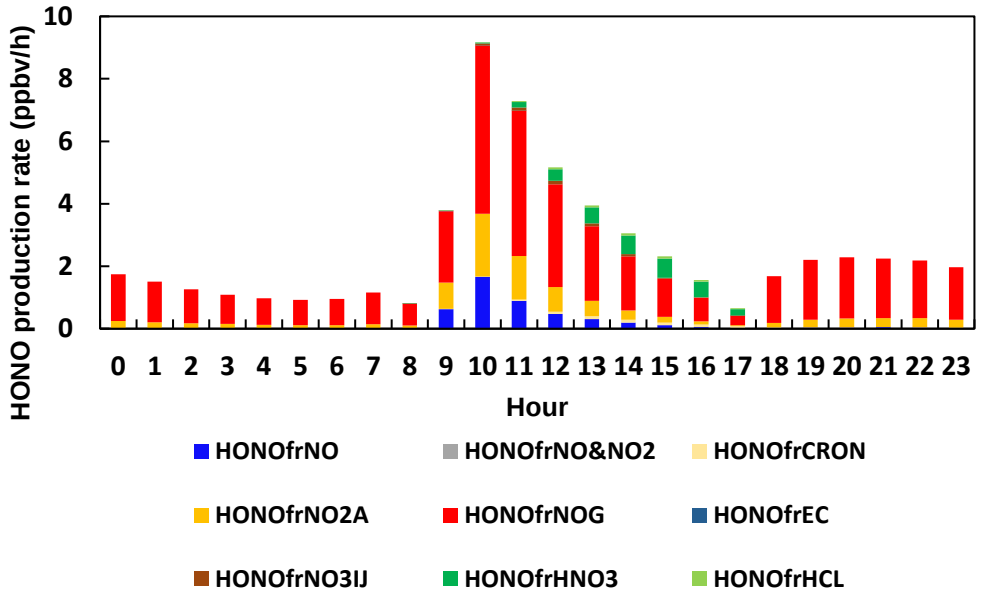

Fig. S7: Surface level integrated reaction rates of the six additional HONO reactions in Beijing December 2015.

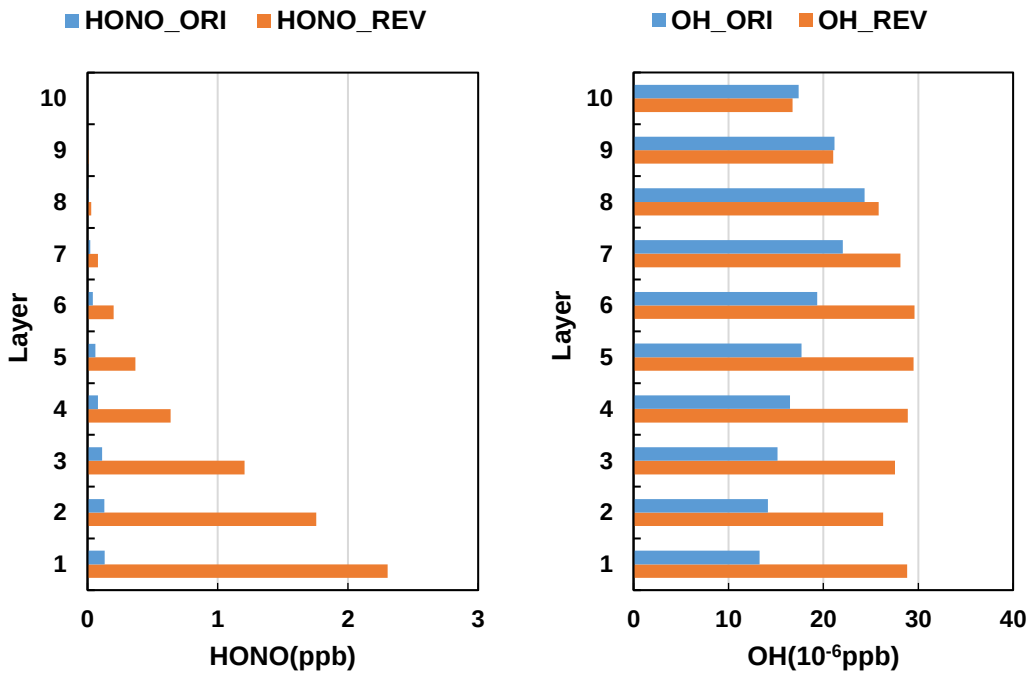

Fig. S8: Vertical profile of HONO and OH in Beijing simulated for ORI (blue bar) and REV (orange bar). Full-layer heights above ground are 36, 73, 146, 294, 445, 675, 1072, 1573, 2103, and 2965 m.

Table S1: A comparison of observed HONO concentrations in China

Station	Time	Equipment	HONO (ppb)	Reference
Heshan	Jan 4-8, 2017	LOPAP	0.2-8.8	(Fu et al., 2019)
Chengdu	Sep 1-Dec 30, 2017	GAC-IC TH-PKU-303	0.3-1	(Wu et al., 2018)
Xi'an	Dec 16-24, 2015	IGAC	0.5-4	(Feng et al., 2018)
Shanghai	May 12-28, 2016	LOPAP	0.3-6	(Cui et al., 2018)
Xianggang	Aug 20-31, 2011	LOPAP	0.45-2.71	(Zhang et al., 2016)
Beijing	Dec 16-23, 2016	custom	3.5±2.7	(Zhang et al., 2019b)
Jinan	Sep 1, 2015-Aug 31, 2016	LOPAP	17-8.36	(Li et al., 2018a)
Beijing	Aug 2-30, 2006	LOPAP	0.06-3	(Zhang et al., 2019a)
Beijing	Sep 22, 2015-Jul 25, 2016	AIM-IC（custom）	1.05-2.27	(Wang et al., 2017)
Beijing	Feb 22-Mar 2, 2014	custom	0.49-3.24	(Hou et al., 2016)
Beijing	Oct 28-Nov 2, 2014	custom	0.54-2.7	(Tong et al., 2016)
Beijing	Dec 7-22, 2015	custom	2.3±1.8	This study

Table S2: The uptake coefficient of NO_2 used in other studies.

γ_{NO2}	reference	γ_{NO2}	reference
1×10^{-6}	(Li et al., 2018a)	8×10^{-6}	(Liu et al., 2019b)
1×10^{-5}	(Fu et al., 2019)	1×10^{-6}	(Liu et al., 2014)
1×10^{-6}	(Ndour et al., 2008)	$2\sim7\times10^{-4}$	(Lu et al., 2018)
1×10^{-7}	(Stemmler et al., 2007)	5×10^{-6}	(Meng et al., 2020)
$10^{-3}\sim10^{-4}$	(Li et al., 2018b)	$1\sim6\times10^{-7}$	(Monge et al., 2010)
1×10^{-6}	(Liu et al., 2019a)	3×10^{-5}	(Spataro et al., 2013)
1×10^{-6}	(Liu et al., 2021)		

Table S3: Average VOC concentrations and reaction rates of VOCS with OH in the ORI and REV models in Beijing

	Conc (ppb)			R_{VOC+OH} (ppt/h)		
	ORI		REV	ORI		REV
Acetaldehyde	2.46	⇒	2.80	58.37	⇒	123.06
Higher-aldehydes	2.79	⇒	2.95	63.18	⇒	124.11
Ethene	14.19	⇐	13.44	53.06	⇒	83.94
Ethane	14.91	⇐	14.89	1.28	⇒	2.46
Ethanol	0.78	⇐	0.75	1.36	⇒	2.39
Formaldehyde	11.63	⇒	12.44	75.56	⇒	163.75

Internal olefin	0.81	⇐	0.69	7.42	⇐	6.98
Isoprene	0.04	=	0.04	1.10	⇐	1.01
Methanol	1.13	=	1.13	0.47	⇒	0.88
Olefin	25.13	⇐	23.30	258.53	⇒	332.31
Paraffin	186.06	⇐	182.60	80.94	⇒	144.42
Monoterpenes	0.03	⇐	0.02	0.35	⇐	0.21
Toluene	17.24	⇐	16.57	51.83	⇒	86.36
Xylene	16.83	⇐	15.84	123.51	⇒	179.99

References

Chan, W.H., Nordstrom, R.J., Calvert, J.G., Shaw, J.H., 1976a. Kinetic study of nitrous acid formation and decay reactions in gaseous mixtures of nitrous acid, nitrogen oxide (NO), nitrogen oxide (NO2), water, and nitrogen. Environmental Science & Technology 10, 674-682.

Chan, W.H., Nordstrom, R.J., Galvert, J.G., Shaw, J.H., 1976b. An IRFTS spectroscopic study of the kinetics and the mechanism of the reactions in the gaseous system, HONO, NO, NO2, H2O. Chemical Physics Letters 37, 441-446.

Cui, L.L., Li, R., Zhang, Y.C., Meng, Y., Fu, H.B., Chen, J.M., 2018. An observational study of nitrous acid (HONO) in Shanghai, China: The aerosol impact on HONO formation during the haze episodes. Sci. Total Environ. 630, 1057-1070.

Czader, B.H., Choi, Y., Li, X., Alvarez, S., Lefer, B., 2015. Impact of updated traffic emissions on HONO mixing ratios simulated for urban site in Houston, Texas. Atmospheric Chemistry and Physics 15, 1253-1263.

Feng, T., Bei, N., Zhao, S., Wu, J., Li, X., Zhang, T., Cao, J., Zhou, W., Li, G., 2018. Wintertime nitrate formation during haze days in the Guanzhong basin, China: A case study. Environmental pollution 243, 1057-1067.

Fu, X., Wang, T., Zhang, L., Li, Q.Y., Wang, Z., Xia, M., Yun, H., Wang, W.H., Yu, C., Yue, D.L., Zhou, Y., Zheng, J.Y., Han, R., 2019. The significant contribution of HONO to secondary pollutants during a severe winter pollution event in southern China. Atmospheric Chemistry and Physics 19, 1-14.

Hou, S., Tong, S., Ge, M., An, J., 2016. Comparison of atmospheric nitrous acid during severe haze and clean periods in Beijing, China. Atmospheric Environment 124, 199-206.

Jaeglé, L., Shah, V., Thornton, J.A., Lopez-Hilfiker, F.D., Lee, B.H., McDuffie, E.E., Fibiger, D., Brown, S.S., Veres, P., Sparks, T.L., Ebben, C.J., Wooldridge, P.J., Kenagy, H.S., Cohen, R.C., Weinheimer, A.J., Campos, T.L., Montzka, D.D., Digangi, J.P., Wolfe, G.M., Hanisco, T., Schroder, J.C., Campuzano-Jost, P., Day, D.A., Jimenez, J.L., Sullivan, A.P., Guo, H., Weber, R.J., 2018. Nitrogen Oxides Emissions, Chemistry, Deposition, and Export Over the Northeast United States During the WINTER Aircraft Campaign. Journal of Geophysical Research: Atmospheres 123, 12,368-312,393.

Kaiser, E.W., Wu, C.H., 1977. A kinetic study of the gas phase formation and decomposition reactions of nitrous acid. The Journal of Physical Chemistry 81, 1701-1706.

Kurtenbach, R., Becker, K., Gomes, J., Kleffmann, J., Lörzer, J., Spittler, M., Wiesen, P., Ackermann, R., Geyer, A., Platt, U., 2001. Investigations of emissions and heterogeneous formation of HONO in a road traffic tunnel. Atmospheric Environment 35, 3385-3394.

Li, D.D., Xue, L.K., Wen, L., Wang, X.F., Chen, T.S., Mellouki, A., Chen, J.M., Wang, W.X., 2018a. Characteristics and sources of nitrous acid in an urban atmosphere of northern China: Results from 1-yr continuous observations. Atmospheric Environment 182, 296-306.
Li, L.J., Hoffmann, M.R., Colussi, A.J., 2018b. Role of Nitrogen Dioxide in the Production of Sulfate during Chinese Haze-Aerosol Episodes. Environmental Science & Technology 52, 2686-2693.
Liang, Y., Zha, Q., Wang, W., Cui, L., Lui, K.H., Ho, K.F., Wang, Z., Lee, S.-c., Wang, T., 2017. Revisiting nitrous acid (HONO) emission from on-road vehicles: A tunnel study with a mixed fleet. J. Air Waste Manage. Assoc. 67, 797-805.
Liu, J., Li, S., Mekic, M., Jiang, H., Zhou, W., Loisel, G., Song, W., Wang, X., Gligorovski, S., 2019a. Photoenhanced Uptake of NO2 and HONO Formation on Real Urban Grime. Environmental Science & Technology Letters.
Liu, J., Liu, Z., Ma, Z., Yang, S., Yao, D., Zhao, S., Hu, B., Tang, G., Sun, J., Cheng, M., Xu, Z., Wang, Y., 2021. Detailed budget analysis of HONO in Beijing, China: Implication on atmosphere oxidation capacity in polluted megacity. Atmospheric Environment 244.
Liu, Y., Han, C., Ma, J., Bao, X., He, H., 2015. Influence of relative humidity on heterogeneous kinetics of NO2 on kaolin and hematite. Physical Chemistry Chemical Physics 17, 19424-19431.
Liu, Y., Lu, K., Li, X., Dong, H., Tan, Z., Wang, H., Zou, Q., Wu, Y., Zeng, L., Hu, M., Min, K.-E., Kecorius, S., Wiedensohler, A., Zhang, Y., 2019b. A Comprehensive Model Test of the HONO Sources Constrained to Field Measurements at Rural North China Plain. Environmental Science & Technology 53, 3517-3525.
Liu, Z., Wang, Y., Costabile, F., Amoroso, A., Zhao, C., Huey, L.G., Stickel, R., Liao, J., Zhu, T., 2014. Evidence of Aerosols as a Media for Rapid Daytime HONO Production over China. Environmental Science & Technology 48, 14386-14391.
Lu, X.C., Wang, Y.H., Li, J.F., Shen, L., Fung, J.C.H., 2018. Evidence of heterogeneous HONO formation from aerosols and the regional photochemical impact of this HONO source. Environ. Res. Lett. 13, 12.
Ma, Q.X., Wang, T., Liu, C., He, H., Wang, Z., Wang, W.H., Liang, Y.T., 2017. SO2 Initiates the Efficient Conversion of NO2 to HONO on MgO Surface. Environmental Science & Technology 51, 3767-3775.
Meng, F., Qin, M., Tang, K., Duan, J., Fang, W., Liang, S., Ye, K., Xie, P., Sun, Y., Xie, C., Ye, C., Fu, P., Liu, J., Liu, W., 2020. High-resolution vertical distribution and sources of HONO and NO₂ in the nocturnal boundary layer in urban Beijing, China. Atmospheric Chemistry and Physics 20, 5071-5092.
Monge, M., D'Anna, B., Mazri, L., Giroir-Fendler, A., Ammann, M., Donaldson, D.J., George, C., 2010. Light changes the atmospheric reactivity of soot. Proceedings of the National Academy of Sciences of the United States of America 107, 6605-6609.
Nakashima, Y., Kajii, Y., 2017. Determination of nitrous acid emission factors from a gasoline vehicle using a chassis dynamometer combined with incoherent broadband cavity-enhanced absorption spectroscopy. Sci. Total Environ. 575, 287-293.
Ndour, M., D'Anna, B., George, C., Ka, O., Balkanski, Y., Kleffmann, J., Stemmler, K., Ammann, M., 2008. Photoenhanced uptake of NO2 on mineral dust: Laboratory experiments and model simulations. Geophysical Research Letters 35.
Oswald, R., Behrendt, T., Ermel, M., Wu, D., Su, H., Cheng, Y., Breuninger, C., Moravek, A., Mougin, E., Delon, C., 2013. HONO emissions from soil bacteria as a major source of atmospheric reactive nitrogen. Science 341, 1233-1235.
Rasool, Q.Z., Bash, J.O., Cohan, D.S., 2019. Mechanistic representation of soil nitrogen emissions in the

241 Community Multiscale Air Quality (CMAQ) model v 5.1. Geosci Model Dev 12, 849-878.
242 Sarwar, G., Roselle, S.J., Mathur, R., Appel, W., Dennis, R.L., Vogel, B., 2008. A comparison of CMAQ
243 HONO predictions with observations from the northeast oxidant and particle study. Atmospheric
244 Environment 42, 5760-5770.
245 Spataro, F., Ianniello, A., Esposito, G., Allegrini, I., Zhu, T., Hu, M., 2013. Occurrence of atmospheric
246 nitrous acid in the urban area of Beijing (China). Sci. Total Environ. 447, 210-224.
247 Stemmler, K., Ndour, M., Elshorbany, Y., Kleffmann, J., D'Anna, B., George, C., Bohn, B., Ammann, M.,
248 2007. Light induced conversion of nitrogen dioxide into nitrous acid on submicron humic acid aerosol.
249 Atmos. Chem. Phys. 7, 4237-4248.
250 Su, H., Cheng, Y., Oswald, R., Behrendt, T., Trebs, I., Meixner, F.X., Andreae, M.O., Cheng, P., Zhang,
251 Y., Pöschl, U., 2011. Soil Nitrite as a Source of Atmospheric HONO and OH Radicals. Science 333, 1616.
252 Svoboda, O., Kubelová, L., Slavíček, P., 2013. Enabling Forbidden Processes: Quantum and Solvation
253 Enhancement of Nitrate Anion UV Absorption. The Journal of Physical Chemistry A 117, 12868-12877.
254 Tong, S., Hou, S., Zhang, Y., Chu, B., Liu, Y., He, H., Zhao, P., Ge, M., 2016. Exploring the nitrous acid
255 (HONO) formation mechanism in winter Beijing: direct emissions and heterogeneous production in
256 urban and suburban areas. Faraday discussions 189, 213-230.
257 Trinh, H.T., Imanishi, K., Morikawa, T., Hagino, H., Takenaka, N., 2017. Gaseous nitrous acid (HONO)
258 and nitrogen oxides (NOx) emission from gasoline and diesel vehicles under real-world driving test
259 cycles. J. Air Waste Manage. Assoc. 67, 412-420.
260 VandenBoer, T.C., Brown, S.S., Murphy, J.G., Keene, W.C., Young, C.J., Pszenny, A.A.P., Kim, S.,
261 Warneke, C., de Gouw, J.A., Maben, J.R., Wagner, N.L., Riedel, T.P., Thornton, J.A., Wolfe, D.E., Dubé,
262 W.P., Öztürk, F., Brock, C.A., Grossberg, N., Lefer, B., Lerner, B., Middlebrook, A.M., Roberts, J.M.,
263 2013. Understanding the role of the ground surface in HONO vertical structure: High resolution vertical
264 profiles during NACHTT-11. Journal of Geophysical Research: Atmospheres 118, 10,155-110,171.
265 Wang, G., Cheng, S., Wei, W., Yang, X., Wang, X., Jia, J., Lang, J., Lv, Z., 2017. Characteristics and
266 emission-reduction measures evaluation of PM2.5 during the two major events: APEC and Parade. The
267 Science of the total environment 595, 81-92.
268 Wormhoudt, J., Wood, E.C., Knighton, W.B., Kolb, C.E., Herndon, S.C., Olaguer, E.P., 2015. Vehicle
269 emissions of radical precursors and related species observed in the 2009 SHARP campaign. J. Air Waste
270 Manage. Assoc. 65, 699-706.
271 Wu, P., Huang, X., Zhang, J., Luo, B., Luo, J., Song, H., Zhang, W., Rao, Z., Feng, Y., Zhang, J., 2018.
272 Characteristics and formation mechanisms of autumn haze pollution in Chengdu based on high time-
273 resolved water-soluble ion analysis. Environmental science and pollution research international.
274 Xu, Z., Wang, T., Wu, J., Xue, L., Chan, J., Zha, Q., Zhou, S., Louie, P.K.K., Luk, C.W.Y., 2015. Nitrous
275 acid (HONO) in a polluted subtropical atmosphere: Seasonal variability, direct vehicle emissions and
276 heterogeneous production at ground surface. Atmospheric Environment 106, 100-109.
277 Zhang, J.W., An, J.L., Qu, Y., Liu, X.G., Chen, Y., 2019a. Impacts of potential HONO sources on the
278 concentrations of oxidants and secondary organic aerosols in the Beijing-Tianjin-Hebei region of China.
279 Sci. Total Environ. 647, 836-852.
280 Zhang, L., Wang, T., Zhang, Q., Zheng, J.Y., Xu, Z., Lv, M.Y., 2016. Potential sources of nitrous acid
281 (HONO) and their impacts on ozone: A WRF-Chem study in a polluted subtropical region. J. Geophys.
282 Res.-Atmos. 121, 3645-3662.
283 Zhang, W.Q., Tong, S.R., Ge, M.F., An, J.L., Shi, Z.B., Hou, S.Q., Xia, K.H., Qu, Y., Zhang, H.X., Chu,
284 B.W., Sun, Y.L., He, H., 2019b. Variations and sources of nitrous acid (HONO) during a severe pollution

episode in Beijing in winter 2016. Sci. Total Environ. 648, 253-262.
Zheng, H., Song, S., Sarwar, G., Gen, M., Wang, S., Ding, D., Chang, X., Zhang, S., Xing, J., Sun, Y., Ji, D., Chan, C.K., Gao, J., McElroy, M.B., 2020. Contribution of Particulate Nitrate Photolysis to Heterogeneous Sulfate Formation for Winter Haze in China. Environmental Science & Technology Letters.
Zhou, X., Gao, H., He, Y., Huang, G., Bertman, S.B., Civerolo, K., Schwab, J., 2003. Nitric acid photolysis on surfaces in low-NOx environments: Significant atmospheric implications. Geophysical Research Letters 30.